Nanoscale control of an interfacial metal–insulator transition at room temperature

C. CEN[1], S. THIEL[2], G. HAMMERL[2], C. W. SCHNEIDER[2], K. E. ANDERSEN[3], C. S. HELLBERG[3], J. MANNHART[2] AND J. LEVY[1]*

[1]Department of Physics and Astronomy, University of Pittsburgh, 3941 O'Hara St., Pittsburgh, Pennsylvania 15260, USA
[2]Experimental Physics VI, Center for Electronic Correlations and Magnetism, Institute of Physics, University of Augsburg, D-86135, Augsburg, Germany
[3]Center for Computational Materials Science, Naval Research Laboratory, Washington, DC 20375, USA
*e-mail: jlevy@pitt.edu

Published online: 2 March 2008; doi:10.1038/nmat2136

Experimental[1–7] and theoretical[8,9] investigations have demonstrated that a quasi-two-dimensional electron gas (q-2DEG) can form at the interface between two insulators: non-polar $SrTiO_3$ and polar $LaTiO_3$ (ref. 2), $LaAlO_3$ (refs 3–5), $KTaO_3$ (ref. 7) or $LaVO_3$ (ref. 6). Electronically, the situation is analogous to the q-2DEGs formed in semiconductor heterostructures by modulation doping. $LaAlO_3/SrTiO_3$ heterostructures have recently been shown[10] to exhibit a hysteretic electric-field-induced metal–insulator quantum phase transition for $LaAlO_3$ thicknesses of 3 unit cells. Here, we report the creation and erasure of nanoscale conducting regions at the interface between two insulating oxides, $LaAlO_3$ and $SrTiO_3$. Using voltages applied by a conducting atomic force microscope (AFM) probe, the buried $LaAlO_3/SrTiO_3$ interface is locally and reversibly switched between insulating and conducting states. Persistent field effects are observed using the AFM probe as a gate. Patterning of conducting lines with widths of ∼3 nm, as well as arrays of conducting islands with densities $>10^{14}$ inch^{-2}, is demonstrated. The patterned structures are stable for >24 h at room temperature.

The success of semiconductors as technological materials is based on three important features: (1) their electrical conductivity can be tuned over a wide range, either by doping or through electric-field effects; (2) insulating layers (SiO_2) can be formed readily, enabling field-effect devices to be fabricated; (3) devices can be scaled to nanoscale dimensions. Oxide materials combine many of the important electronic properties of semiconductors[10,11] with extra emergent phenomena, such as interfacial superconductivity[12], strain-driven ferroelectricity[13], interfacial ferromagnetism[14] and colossal magnetoresistance[15].

The discovery of metallic and superconducting interfaces between insulating oxides has led to many subsequent investigations about the origin of this effect, and in particular the role played by oxygen vacancies[16,17]. In samples that are heated to ∼800 °C in high vacuum (order of 10^{-6} mbar), oxygen defects are created in the $SrTiO_3$ substrates which n-dope the material, regardless of the presence of a $LaAlO_3$ layer[18–21]. For samples grown under oxygen pressures $\geq 10^{-5}$ mbar, as in the experiments described here, the interfacial conductance is dominated by the potential profile generated between the $SrTiO_3/LaAlO_3$ interface and the top $LaAlO_3$ surface. Thiel *et al.* recently found that for samples with 3 unit cells of $LaAlO_3$, a bistable metal–insulator transition can be tuned with a voltage applied between the $LaAlO_3/SrTiO_3$ interface and the bottom $SrTiO_3$ substrate[10], suggesting a role played by both the polar discontinuity and residual oxygen vacancies in the $SrTiO_3$.

Although oxides provide a wealth of opportunities for probing the rich physics of correlated electronic systems, for technological applications it is essential to scale device concepts to nanoscale dimensions. Ferroelectric field effects at ∼350 nm scales have been reported for oxide heterostructures[22]. Here, we present a technique that can dynamically define at room temperature nanoscale conducting structures at the interface of two insulating oxides, $LaAlO_3$ and $SrTiO_3$, through reversible control of a localized metal–insulator transition. Both isolated and continuous conducting features with length scales well below 5 nm are demonstrated. Strong nonlinear electric-field effects are also observed. We suggest one possible theoretical explanation for this behaviour in terms of the creation of oxygen vacancies in the topmost $LaAlO_3$ surface.

The material system investigated here consists of 3 unit cells of $LaAlO_3$, grown at 770 °C in an O_2 pressure of 6×10^{-5} mbar by pulsed laser deposition on a TiO_2-terminated insulating $SrTiO_3$ substrate[10]. The samples were cooled in 400 mbar of O_2 with a 1 h oxidation step at 600 °C. Several samples were prepared under identical conditions and characterized. One of these samples was used for the studies described here. All measurements are carried out in air at 295 K. The sample is maintained in a dark environment to suppress carrier photoexcitation in $SrTiO_3$ (bandgap ∼ 3.2 eV). A set of electrodes, in contact with the interface and spaced $D_0 = 150\,\mu$m apart, is fabricated using the techniques described in ref. 10.

A conducting atomic force microscope (AFM) tip, in contact with the top $LaAlO_3$ surface and biased at V_{tip} with respect to the interface, produces an interfacial metallic ($V_{tip} > 0$) or insulating ($V_{tip} < 0$) state directly below the area of contact. Note that V_{tip} is applied between the top $LaAlO_3$ surface and the $LaAlO_3/SrTiO_3$ interface; in the experiments of Thiel *et al.*[10], the voltage was

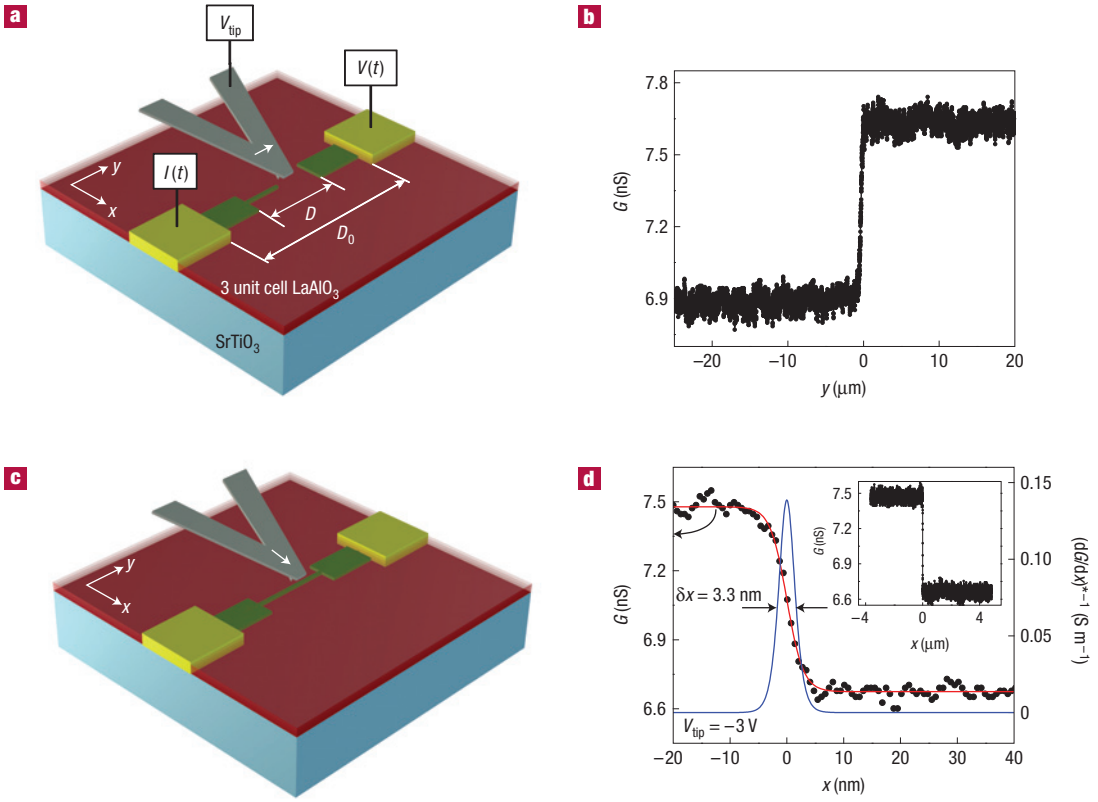

Figure 1 Writing and erasing nanowires at the $LaAlO_3$/$SrTiO_3$ interface. a, Schematic diagram of the experimental set-up for writing a conducting wire. A voltage-biased AFM tip is scanned from one electrode towards a second one in contact mode. The tip generates an electric field that causes a metallic q-2DEG to form locally at the interface under the route of the tip. **b**, Conductance between the two electrodes measured with a lock-in amplifier as a function of the tip position while writing a conducting wire with 3 V bias applied to the tip. A steep increase in conductance occurs when the tip reaches the second electrode. **c**, Schematic diagram of the experimental set-up for cutting a conducting wire. The negatively biased AFM tip moves in contact mode across the conducting wire. The tip erases the metallic q-2DEG locally when it crosses the conducting wire. The conductance between two electrodes is monitored as the tip scans over the wire. **d**, Conductance between the two electrodes measured as a function of the tip position across the wire, while cutting the wire with the tip biased at −3 V. A sharp drop in conductance occurs when the tip passes the wire. The inset shows the conductance measured over the entire 8 μm scan length. The decrease in conductance can be fitted to a profile $G(x) = G_0 - G_1 \tanh(x/h)$ with best-fit parameters given by $G_0 = 7.1$ nS, $G_1 = 0.40$ nS and $h = 2.9$ nm. The deconvolved differential conductance $(dG/dx)^{*-1}$ showing a full-width at half-maximum $\delta x = 3.3$ nm is also plotted.

applied between the interface and the bottom $SrTiO_3$ substrate surface. For the experiment described below, the gap between the conducting electrodes is first reduced to $D = 40$ μm by 'writing' (that is, raster-scanning at $V_{tip} = +10$ V) two rectangular pads (Fig. 1a). The electric conductance between the two electrodes is monitored using a lock-in amplifier. The AFM tip, now biased at $V_{tip} = +3$ V, writes a line by scanning from one electrode to the other. As the tip reaches the second electrode, a pronounced and abrupt conductance increase $\Delta G \approx 0.8$ nS is observed (Fig. 1b). This increase is not associated with any observed topographic changes of the structure, nor is it affected by subsequent imaging by an electrically isolated or grounded probe.

To provide a measure of the transverse dimension of the conducting wire, and to demonstrate that the writing process is reversible, the wire is subsequently 'cut' with a reverse voltage $V_{tip} = -3$ V (Fig. 1c). As the AFM tip crosses the wire, the conductance decreases abruptly by $\Delta G \approx -0.8$ nS (Fig. 1d). Assuming the erasure process to have a resolution comparable to the writing process, the deconvolved differential profile $(dG/dx)^{*-1}$ thus exhibits a full-width at half-maximum of $\delta x = 3.3$ nm. Subsequent writing with positive voltages over the affected area (for example, $V_{tip} = +3$ V) restores the conductance of the wire. The wire width depends sensitively on V_{tip}, increasing by three orders of magnitude as V_{tip} is raised from 3 V to 10 V. Test measurements were carried out over a 24 h interval and showed that the wires remain stable over that time frame.

The written wires are highly sensitive to externally applied electric fields. Figure 2a shows the current–voltage (I–V) characteristics of a 20-μm-long wire, created with $V_{tip} = 10$ V, that has been perturbed by the AFM probe with varying voltages. The AFM probe functions much like the gate of a ferroelectric field-effect transistor, except that the probe can be scanned. For each curve, the AFM probe is set to a voltage V_{gate} and scanned once across the wire. Afterwards, the in-plane current $I_{\parallel}$ is measured (using a picoammeter referenced to virtual ground) as a function of the voltage V_{sd} applied to one electrode. For low $|V_{gate}|$, the wire conductance is unaffected. However, as the tip bias becomes more negative, the wire becomes insulating and conducts only above a finite bias. This turn-on bias increases monotonically with $|V_{gate}|$. Eventually the I–V curve becomes asymmetric, the probable origin of which is an asymmetry in the insulating barrier profile, produced by unequal electric fields on both sides of the AFM tip.

It is also possible to write isolated conducting islands or 'dots' by applying voltage pulses $V_{tip}(t)$ with amplitude V_{pulse} and duration

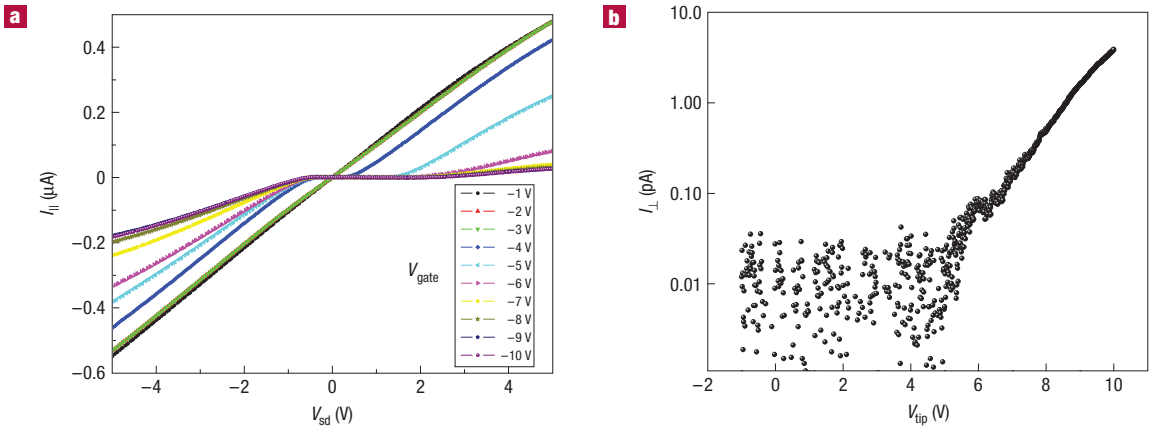

Figure 2 Current–voltage characteristics of $LaAlO_3$ / $SrTiO_3$ interface. a, Current $I_{\parallel}$ versus 'source–drain' voltage V_{sd} of a 20-μm-long q-2DEG wire with a potential barrier near the centre, created with a negative 'gate' bias V_{gate}. The barrier is created using the method shown in Fig. 1c. Different colours represent different tip biases. When the line is interrupted with a sufficiently large tip bias, the *I–V* characteristic becomes strongly nonlinear. Conducting behaviour is observed at large d.c. source voltages. **b**, AFM tip current $I_{\perp}$ versus tip voltage V_{tip} with respect to grounded interface.

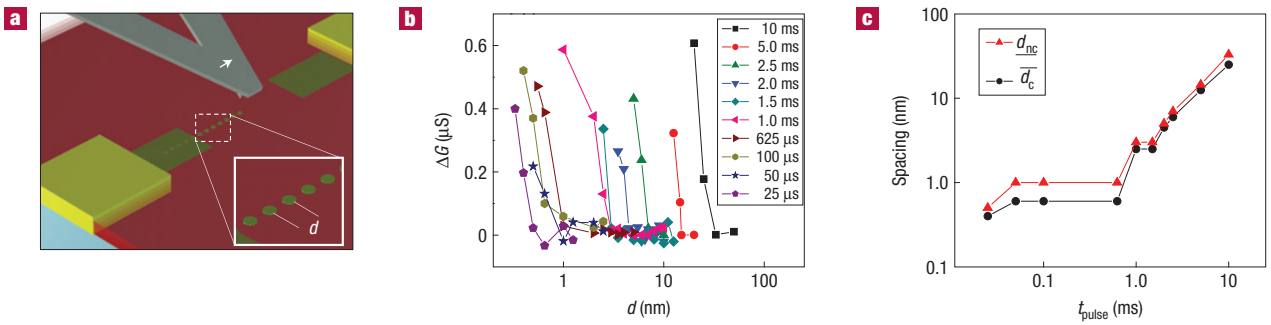

Figure 3 Measuring the limits of conducting island density. a, Schematic diagram showing a linear array of dots written with voltage pulses. **b**, Conductance change as the array is connected to electrodes, for various spacings between dots and different pulse durations. **c**, Plot of minimum dot spacing for which the array is non-conducting $\underline{d_{nc}}$ and the maximum dot spacing for which the array is conducting $\overline{d_c}$, presented as a function of pulse duration t_{pulse}.

t_{pulse} to the tip while keeping the tip at a fixed position. During pulsed writing the two electrodes are grounded. The size of the dots depends on both V_{pulse} and t_{pulse}. For simplicity, we keep $V_{pulse} = 10\,V$ fixed and vary t_{pulse} to change the size of the dots. To determine the effective size of the dots, linear arrays of dots are created with various separations d (Fig. 3a). After writing the arrays, the ends of the arrays are contacted by writing conducting electrodes, which are separated by $D = 1\,\mu m$. As the contacts are being written, the conductance between the two electrodes is monitored using a lock-in amplifier. If the spacing between the dots is greater than the dot diameter, the dots will not overlap and no increase in conductance will be observed. Once the spacing becomes equal to or smaller than the dot diameter, the linear array will form a conducting wire, manifested as an abrupt increase in conductance between the two electrodes (ΔG), once the wire is attached. For each pulse duration, a sharp metal–insulator transition is observed as the dot spacing is reduced (Fig. 3b). The smallest non-conducting spacing $\underline{d_{nc}}$ and the largest conducting spacing $\overline{d_c}$ are plotted as a function of t_{pulse} (Fig. 3c). The critical spacing for conduction d_c is bound by these two measured quantities ($\underline{d_{nc}} > d_c \geq \overline{d_c}$) and scales linearly with pulse duration until pulse durations $t_{pulse} < 1\,ms$ are used. Below that threshold, the critical spacing levels off at $\overline{d_c} \sim 1\,nm$.

The exceptionally small size of the features results from the nature of the writing process. The voltage-biased AFM tip produces large local electric fields ($E \sim V_{tip}/L$) across the $L = 1.2$-nm-thick $LaAlO_3$ barrier. Tunnelling measurements carried out between the conducting AFM tip and the $LaAlO_3/SrTiO_3$ interface (Fig. 2b) show that for voltages $V_{tip} > V_t \sim 6\,V$ the current $I_{\perp}$ is governed by Fowler–Nordheim tunnelling between the tip and the interface. Tunnelling takes place over an area the radius of which may be estimated by assuming hertzian contact[23] to be $r_{contact} = 1.2\,nm$. Writing at voltages smaller than V_t is possible, but not via direct tunnelling. Writing of conducting wires at, for example, $V_{tip} = 3\,V$ is only achieved if a conducting path already exists to one of the electrodes (Fig. 1). Isolated conducting regions cannot be written with $V_{tip} < V_t$.

Because there is no strong anisotropy present in the $SrTiO_3$ or $LaAlO_3$, the minimum lateral feature size is expected to be comparable to the scale for vertical confinement of the mobile electrons. Indeed, the smallest dot spacing observed is comparable to the observed thickness $\delta z = 2\,nm$ for the quasi-two-dimensional

electron gas (q-2DEG) of a closely related system, $LaTiO_3/SrTiO_3$ (ref. 2). Using $\delta x = \delta z = 2$ nm and $l = 1\,\mu$m, we obtain a resistivity for the wires $\rho = \delta x \delta z / Gl = 2 \times 10^{-3}\,\Omega$ cm, which is close to the Mott–Ioffe–Regel threshold.

We also carried out similar experiments on bare $SrTiO_3$, 2 unit cells of $LaAlO_3$ on $SrTiO_3$ and 4 unit cells of $LaAlO_3$ on $SrTiO_3$, the details of which are described in the Supplementary Information. Experiments show that only in the sample with 3 unit cell $LaAlO_3$ layer thickness[10] conducting regions can be created and cleared at an insulating interface.

To provide insight into the electronic structure and stability of the metallic and insulating state of $LaAlO_3/SrTiO_3$, we carried out first-principles density functional theory calculations of $LaAlO_3$ films on $SrTiO_3$ substrates. These calculations do not consider possible correlation effects at the interface[8,9]. Computational details are given in the Supplementary Information. Considering the experiment, an n-type (LaO/TiO_2) interface is used. The top surface of the $LaAlO_3$ is assumed to be clean and terminated with an AlO_2 layer. For 3-unit-cell-thick films, two structures are predicted to be stable. As shown in Supplementary Information, Fig. S1, the two structures differ by the presence of oxygen vacancies on the surface. The two structures are predicted to have dramatically different electrical properties. The 'ideal' film without vacancies (see Supplementary Information, Fig. S1a) is insulating. Removing oxygen ions from the $LaAlO_3$ surface layer (see Supplementary Information, Fig. S1b) accompanies the accumulation of mobile electrons at the interface.

The predicted behaviour of the two structures can be understood by examining the local density of states (LDOS), shown in Fig. 4, and the schematic band diagrams derived from the LDOS (see Supplementary Information, Fig. S2). The ideal film has a strong electric field in the $LaAlO_3$, but at 3 unit cells the heterostructure is insulating. With one extra $LaAlO_3$ unit cell the system becomes metallic[10]. The strong field is energetically expensive; by including oxygen vacancies at the $LaAlO_3$ surface, we find that the electric field can be reduced or completely compensated. Such $LaAlO_3$ oxygen vacancies contribute electrons to the conduction band, and the lowest-energy conduction band states are in the $SrTiO_3$ (see Supplementary Information, Fig. S2a). At a density of $n_V = 1/4$ vacancies per 1×1 surface cell, the formal charge of the surface has changed from $-1e$ for the ideal AlO_2 surface to $-e/2$ for the $AlO_{1.75}$ surface. The 1/2 electron per unit cell populates the $SrTiO_3$ conduction band on the opposite side of the $LaAlO_3$ film. In this scenario, the oxygen vacancies in the $LaAlO_3$ and conduction electrons of the $SrTiO_3$ together cancel the field in the $LaAlO_3$, as seen in Fig. 4 and Supplementary Information, Fig. S2b. The only metallic region in this system is the $SrTiO_3$ at the $LaAlO_3/SrTiO_3$ interface—the surface remains insulating.

In this model, switching between the two stable structures requires removing oxygen from the $n_V = 0$ surface and adding oxygen to the $n_V = 1/4$ surface. There are probably significant kinetic barriers to these processes, which the charged AFM tip may be able to overcome. Thus, without ruling out other mechanisms such as charging of trap states, this model suggests the possibility that a positively charged AFM tip 'writes' metallic wires at the interface by removing oxygen from the $LaAlO_3$ surface, and a negatively charged AFM tip 'erases' metallic regions by facilitating adsorption of oxygen or other anions. The theoretical calculations described here do not explain how oxygen might be removed or restored to the $LaAlO_3$ surface; they simply predict that a metal–insulator transition will result from this process. Further experimental and theoretical study is required to provide further insight into the physical mechanism that governs this effect.

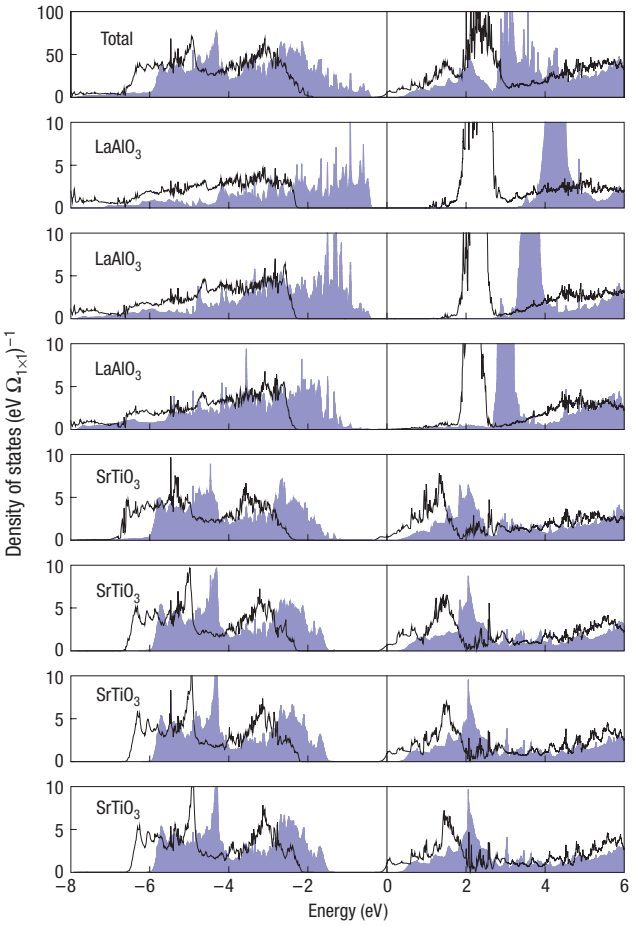

Figure 4 Calculated LDOS of $LaAlO_3/SrTiO_3$ for 'ideal' and reduced $LaAlO_3$ surfaces for each layer in the 3 unit cell $LaAlO_3$ film and for the first four unit cells of the $SrTiO_3$ substrate. The solid blue curve corresponds to the 'ideal' film, whereas the black curve corresponds to the film with surface oxygen vacancies. The ideal film is insulating and has a strong electric field in the $LaAlO_3$. With oxygen vacancies in the $LaAlO_3$ surface, the field is compensated, and 0.5 electrons per 1×1 unit cell enter the $SrTiO_3$ conduction states.

The ability to pattern reversibly high-mobility electron gases at nanoscale dimensions provides new ground to develop devices for ultrahigh-density information storage and processing. Integration with silicon-based devices is possible, as shown by reports of high-quality $SrTiO_3/Si$ heterostructures produced by molecular-beam epitaxy[24].

Received 25 May 2007; accepted 30 January 2008; published 2 March 2008.

References

1. Schneider, C. W., Thiel, S., Hammerl, G., Richter, C. & Mannhart, J. Microlithography of electron gases formed at interfaces in oxide heterostructures. *Appl. Phys. Lett.* **89**, 122101 (2006).
2. Ohtomo, A., Muller, D. A., Grazul, J. L. & Hwang, H. Y. Artificial charge-modulation in atomic-scale perovskite titanate superlattices. *Nature* **419**, 378–380 (2002).
3. Ohtomo, A. & Hwang, H. Y. A high-mobility electron gas at the $LaAlO_3/SrTiO_3$ heterointerface. *Nature* **427**, 423–426 (2006).
4. Ohtomo, A. & Hwang, H. Y. Corrigendum: A high-mobility electron gas at the $LaAlO_3/SrTiO_3$ heterointerface. *Nature* **441**, 120 (2006).
5. Huijben, M. *et al.* Electronically coupled complementary interfaces between perovskite band insulators. *Nature Mater.* **5**, 556–560 (2006).
6. Hotta, Y., Susaki, T. & Hwang, H. Y. Polar discontinuity doping of the $LaVO_3/SrTiO_3$ interface. *Phys. Rev. Lett.* **99**, 236805 (2007).
7. Kalabukhov, A., Gunnarsson, R., Claeson, T. & Winkler, D. Electrical transport properties of polar heterointerface between $KTaO_3$ and $SrTiO_3$. Preprint at <http://arxiv.org/abs/cond-mat/0704.1050> (2007).
8. Okamoto, S., Millis, A. J. & Spaldin, N. A. Lattice relaxation in oxide heterostructures: $LaTiO_3/SrTiO_3$ superlattices. *Phys. Rev. Lett.* **97**, 056802 (2006).

9. Pentcheva, R. & Pickett, W. E. Charge localization or itineracy at $LaAlO_3/SrTiO_3$ interfaces: Hole polarons, oxygen vacancies, and mobile electrons. *Phys. Rev. B* **74**, 035112 (2006).
10. Thiel, S., Hammerl, G., Schmehl, A., Schneider, C. W. & Mannhart, J. Tunable quasi-two-dimensional electron gases in oxide heterostructures. *Science* **313**, 1942–1945 (2006).
11. Ahn, C. H., Triscone, J.-M. & Mannhart, J. Electric field effect in correlated oxide systems. *Nature* **424**, 1015–1018 (2003).
12. Reyren, N. *et al.* Superconducting interfaces between insulating oxides. *Science* **317**, 1196–1199 (2007).
13. Haeni, J. H. *et al.* Room-temperature ferroelectricity in strained $SrTiO_3$. *Nature* **430**, 758–761 (2004).
14. Brinkman, A. *et al.* Magnetic effects at the interface between non-magnetic oxides. *Nature Mater.* **6**, 493–496 (2007).
15. Helmolt, R. v., Wecker, J., Holzapfel, B., Schultz, L. & Samwer, K. Giant negative magnetoresistance in perovskite like $La_{2/3}Ba_{1/3}MnO_x$ ferromagnetic films. *Phys. Rev. Lett.* **71**, 2331–2333 (1993).
16. Levi, B. G. Interface between nonmagnetic insulators may be ferromagnetic and conducting. *Phys. Today* **60**, 23–27 (2007).
17. Eckstein, J. N. Oxide interfaces: Watch out for the lack of oxygen. *Nature Mater.* **6**, 473–474 (2007).
18. Schooley, J. F., Hosler, W. R. & Cohen, M. L. Superconductivity in semiconducting $SrTiO_3$. *Phys. Rev. Lett.* **12**, 474–475 (1964).
19. Siemons, W. *et al.* Origin of charge density at $LaAlO_3$ on $SrTiO_3$ heterointerfaces: Possibility of intrinsic doping. *Phys. Rev. Lett.* **98**, 196802 (2007).
20. Kalabukhov, A. *et al.* Effect of oxygen vacancies in the $SrTiO_3$ substrate on the electrical properties of the $LaAlO_3/SrTiO_3$ interface. *Phys. Rev. B* **75**, 121404 (2007).
21. Herranz, G. *et al.* High mobility in $LaAlO_3/SrTiO_3$ heterostructures: Origin, dimensionality, and perspectives. *Phys. Rev. Lett.* **98**, 216803 (2007).
22. Ahn, C. H. *et al.* Local, nonvolatile electronic writing of epitaxial $Pb(Zr_{0.52}Ti_{0.48})O_3/SrRuO_3$ heterostructures. *Science* **276**, 1100–1103 (1997).
23. Frammelsberger, W., Benstetter, G., Kiely, J. & Stamp, R. C-AFM-based thickness determination of thin and ultra-thin SiO_2 films by use of different conductive-coated probe tips. *Appl. Surf. Sci.* **253**, 3615–3626 (2007).
24. Li, H. *et al.* Two-dimensional growth of high-quality strontium titanate thin films on Si. *J. Appl. Phys.* **93**, 4521–4525 (2003).
25. Perdew, J. P., Burke, K. & Ernzerhof, M. Generalized gradient approximation made simple. *Phys. Rev. Lett.* **77**, 3865–3868 (1996).
26. Kresse, G. & Furthmüller, J. Efficient iterative schemes for ab initio total-energy calculations using a plane-wave basis set. *Phys. Rev. B* **54**, 11169–11186 (1996).
27. Kresse, G. & Joubert, D. From ultrasoft pseudopotentials to the projector augmented-wave method. *Phys. Rev. B* **59**, 1758–1775 (1999).
28. Blöchl, P. E. Projector augmented-wave method. *Phys. Rev. B* **50**, 17953–17979 (1994).
29. Nakagawa, N., Hwang, H. Y. & Muller, D. A. Why some interfaces cannot be sharp. *Nature Mater.* **5**, 204–209 (2006).
30. Jenkins, S. J. Ternary half-metallics and related binary compounds: Stoichiometry, surface states, and spin. *Phys. Rev. B* **70**, 245401 (2004).

Acknowledgements

We gratefully acknowledge helpful interactions and discussions with T. Kopp and S. K. Streiffer. Computations were carried out at the DoD Major Shared Resource Centers. This work was supported by DARPA DAAD-19-01-1-0650, NSF DMR-0704022, the DFG (SFB 484), the EC (Nanoxide) and the ESF (THIOX).
Correspondence and requests for materials should be addressed to J.L.
Supplementary Information accompanies this paper on www.nature.com/naturematerials.